energies

MDPI

Article

Dual Battery Storage Technique for Remote, Location-Based Solar PV System and Standalone Applications

Vellarivelli Balasubramani Thurai Raaj [1], Srinivasa Rao Gorantla [2], Dinesh Karunanidy [3], Ankur Dumka [4], Rajesh Singh [5], Mamoon Rashid [6,*], Yasser Albagory [7] and Sultan S. Alshamrani [8]

1 Department of Electrical and Electronics Engineering, Madanapalle Institute of Technology & Science, Madanapalle 517325, India; info2vb@gmail.com
2 Department of Electrical and Electronics Engineering, VFSTR, Guntur 522213, India; srn.gorantla@gmail.com
3 Department of Computer Science and Technology, Madanapalle Institute of Technology & Science, Madanapalle 517325, India; drdineshk@mits.ac.in
4 Department of Computer Science and Engineering, Women's Institute of Technology, Dehradun 248007, India; ankurdumka2@gmail.com
5 Division of Research & Innovation, Uttaranchal University, Dehradun 248007, India; rajeshsingh@uttaranchaluniversity.ac.in
6 Department of Computer Engineering, Faculty of Science and Technology, Vishwakarma University, Pune 411048, India
7 Department of Computer Engineering, College of Computers and Information Technology, Taif University, P.O. Box 11099, Taif 21944, Saudi Arabia; y.albagory@tu.edu.sa
8 Department of Information Technology, College of Computer and Information Technology, Taif University, P.O. Box 11099, Taif 21944, Saudi Arabia; susamash@tu.edu.sa
* Correspondence: mamoon.rashid@vupune.ac.in; Tel.: +91-7814346505

Citation: Thurai Raaj, V.B.; Gorantla, S.R.; Karunanidy, D.; Dumka, A.; Singh, R.; Rashid, M.; Albagory, Y.; Alshamrani, S.S. Dual Battery Storage Technique for Remote, Location-Based Solar PV System and Standalone Applications. *Energies* **2022**, *15*, 2748. https://doi.org/10.3390/en15082748

Academic Editors: Gianfranco Chicco, Andrea Mazza and Djaffar Ould-Abdeslam

Received: 21 February 2022
Accepted: 5 April 2022
Published: 8 April 2022

Abstract: Nowadays, the usage of renewable energy resources (RER) is growing rapidly, but at the same time, the effective utilization of RER is also a challenging task. For the better usage of RER and the reduction of loss, the dual battery storage is proposed. The main aim of this work is to focus on the design and implementation of a reliable and renewable power generating system under a robust situation, along with a battery storage system. The perturb and observe (P&O) maximum power point tracking (MPPT) technique has been applied to improve the solar photovoltaic power production. In addition, the dual battery storage system is being introduced to improve the life cycle of the primary storage system. The proposed dual storage system is highly preferable for remote, location-based application systems, space applications and military operations. In the dual battery storage system, the batteries are working effectively with a good lifespan, when compared with the existing methods. To determine the state of charge (SOC) and depth of discharge (DOC), those batteries' input charging and discharging levels were monitored closely. MATLAB Simulink (R2013) is used for simulation; finally, a real-time, three-phase inverter was designed and validated. Under this dual battery storage mode, the life time of battery is improved.

Keywords: renewable energy; boost converter; dual battery; state of charge (SOC); depth of charge (DOC); battery charge controller and inverter

1. Introduction

Nowadays, solar power generation plays a vital role in industrial as well as domestic applications. It is a cheap, pollution-free (noise and air) and green energy resource. As per the Ministry of New and Renewable Energy (MNRE), India, the government of India states that the average availability of solar irradiation in the southern part of India is 1266.52 W/m^2. This irradiation is sufficient to produce an average of 5 kWh of electrical power per day by implementing 1 kWp (availability of 5.5-h solar irradiation) through a solar plant. The government of India plans to produce 20 GW of electric power from solar energy by the year 2020. In 2017, the power sector added 167 GW of renewable

energy capacity globally; a robust growth of 8.3% over the previous year was seen. Figure 1 clearly shows the implementation of solar PV power generation in India. Renewable power generation accounted for an estimated one quarter of the total global power generation, a new record. New records were also set for solar and wind installation, with the additions of 94 GW in solar photovoltaic (PV) power and 47 GW in wind power, including 4 GW of offshore wind power.

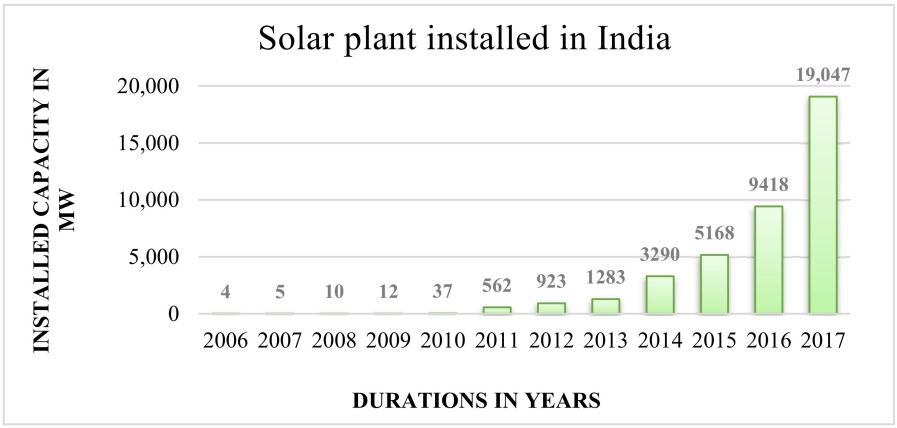

Figure 1. Total installed capacity of solar power sources in India: 2017.

To improve the voltage gain, a single-phase, solar powered inverter is coupled with a capacitor and an inductor with an inverter circuit; moreover, it has a common ground between the input and the output. The overall voltage gain is more than two; similarly, a half-bridge switched boost inverter is also proposed for voltage. Through this method, the inverter can operate in different load conditions [1,2]. The inverter gate pulses play a main role in harmonics generation and reactive power generation; by controlling these input gate pulses, the output parameter will come under control. For that, the MP-PWM technique is proposed in the active filter [3]. To store high-power density, two different categories of storage devises are used in the solar power generation scheme, along with a fuzzy logic controller system [4]. The author [5] designed the dual-ion battery (DIB) to increase its energy density and to handle power density in a faster way. The method used in [6] enhances the DIB by developing new structural design electrodes. Under a dynamic condition, partial shading creates an unexpected error in solar photovoltaic (PV) energy conversion, which [7] provided a solution. In this condition, the flower pollination algorithm (FPA) was applied to find a suitable solution for getting the maximum possible power. The FPA is classified into two groups based on pollination, i.e., the abiotic process, which has its own self-pollination and the biotic process, which means cross-pollination [8]. The steady state oscillation is achieved by the FPA, and finally, the author compares the output with various methods, such as ANN and FUZZY. A single sensor type MPPT (maximum power point tracking) is used as a solution for partial shading in solar photovoltaics. The human psychology optimization (HPO) algorithm controls the entire hardware of the proposed system. A current sensor measured the load current and fed it to the controller. The HPO is nothing but a positive decision at all time—a positive-thinking or goal-oriental person always creates positive energy around his/her surroundings. HPO works based on this statement. It has four factors: excitement, self-motivation, inspiration and lesson. The drawback of this proposal is its possibility to consider a negative value as a positive reference [9,10].

The hill climbing (HC) method is meant for overcoming the uniform solar irradiance problem in solar PV energy conversion. HC is used to improve the output of the solar system by calculating the power differences of two consecutive cycles and by detecting the solar irradiance fault occurrence. Based on the fault detection, a pattern structure is marked in each step. Finally, it will fix the maximum power point. The existing model failed when

multishading occurred at different places [11,12]. Fuzzy logic with maximum dual power point tracking is implemented for attaining the maximum solar radiation. 'Perturb and observe' is integrated with new fuzzy logic in this system, and fuzzy is designed with a five-membership function; the TMS320F 28335 processor controls all parameters [13,14]. The system works towards attaining a steady state stability, and at the same time, it reduces the oscillation. The drawback of this proposal is that it required a high cost for hardware implementation [15,16].

The beta method is used to produce the highest power output from solar PV. In addition, it ensures the tracking time to the maximum power point when compared with any other method. It considers all environment factors, such as temperature, light intensity, weather changes and irradiance. The zero-oscillation perturbation and observation methods have three midpoint-level perturbation; by changing the duty cycle, they maintain the maximum power at the output point. A dSPACE controller produces a control signal and controls the entire system [17,18]. A hybrid Weibull pare (WP) to sine-cosine optimization (SCO) MPPT is implemented for a dynamic and steady state condition. It can find a solution with less steps; under the partially shaded condition, the boost converter is connected to a solar PV and the load. The entire work plan is divided into two modes: first, the SCO finds a place for all the variables; later, the WP updates the required location. The drawback of this project is that it has a charging battery alone; moreover, it failed to validate with nonlinear load [19,20].

For four-wire, three-phase, two-stage, grid-connected solar PV, the boost converter was designed in the first level to get the maximum power generation. The DAND algorithm is introduced for maximum power point tracking; it has a set of multipliers, integrators and summers per phase. The simulation designed for the 25 kW dSPACE controller is used in hardware implementation. It has a solution for load balancing, reactive power compensation and harmonics mitigation [21–23]. The distributed MPPT (DMPPT) technique is implemented to solve multipartial shading; DMPPT has two main divisions: a full power processing structure and a differential power processing structure [24]. This focuses the differential power processing by testing under various topologies, but it has a drawback, which is its efficiency. The Qatar National Research Fund supported this project under the NPRP-EP grant. The author made an investigation on various renewable generating processes, from which he concluded that solar is the best among all other renewable energy sources [25–27]. Moreover, he conducted research on solar energy conversion under two categories: first, generating power from a solar heat energy scheme, including a solar heat collector, steam generator, steam turbine and generator and second, generating power from a direct solar PV-generating scheme under different conditions [28].

A power electronics tool is used to collect electrical energy from renewable energy resources. Before designing a power electronics system, we have to analyse factors such as efficiency, durability of power devices and risk reliability [29,30]. DfR technology was applied here to examine failure identification, strength analysis, strength modelling and reliability mapping of tools [31,32]. A mission profile of the system was examined by various treatments conducted on the tools, and the lifetime was found. The drawback of this paper is related to the design of the power electronics applications [33,34]. To overcome these drawbacks, the dual battery storage system is introduced, and its block diagram is shown in Figure 2. The proposed method controls the charge cycle of the battery, so the lifetime of the battery is increased, and the effective utilization of RER is also achieved.

The rest of the paper is organised as follows: Section 2 covers the proposed method and its detailed discussion, Section 3 deals with solar cell design and the Simulink model, Section 4 discusses the hardware setup of the inverter with its detail control circuits and the results for both hardware and Simulink under the corresponding sections, and finally, Section 5 covers the conclusion.

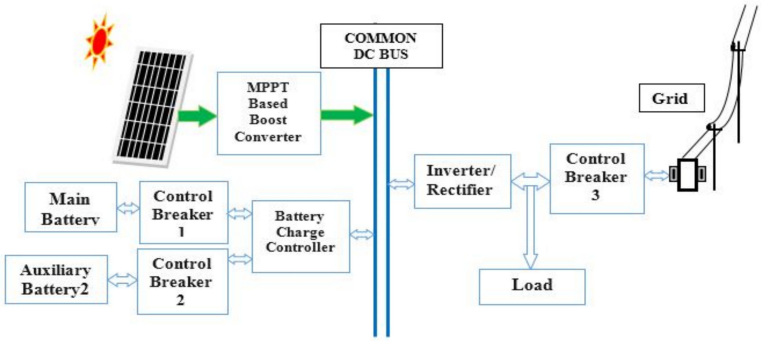

Figure 2. Proposed solar power generation scheme with dual battery storage systems.

2. Proposed Method

In the proposed dual battery operation, the first battery (B1) acts as a primary storage device, and another battery (B2) acts as a standby storage unit. The dual battery algorithm is proposed to control these two batteries. For that, the state of charge (SOC) of two batteries are continuously monitored by using two identical circuits. To avoid ADC errors, identical circuits are used. Based on the SOC percentage and the pervious operating mode, the controller decides the mode of the battery.

In real time, a dsPIC microcontroller is used to load the dual battery algorithm. It has an inbuilt, six-channel 10-bit ADC. The proposed general block diagram is shown in Figure 2. Table 1 explains the mode of operations involved in this system.

Table 1. Parameter-based logical operation for the proposed system.

Solar PV	SOC of Battery 1	SOC of Battery 2	Load Position	Grid Position	Power Source
ON	Max charge	Not fully charged	ON	Ideal	Solar PV
OFF	Max charge	Not fully charged	ON	Ideal	Battery 1
OFF	Low charge	Not fully charged	ON	Ideal	Battery 2
OFF	Charge from grid	Charge from grid	ON	Import	Grid
ON	Max charge	Max charge	OFF	Export	Ideal

Equation (1) expresses the initial condition of batteries:

$$\text{At initial condition} \begin{cases} SOC_1 >= 96\% \\ SOC_2 >= 96\% \end{cases} \quad (1)$$

Equation (2) expresses the condition to set battery 1 as an alternative source to the load. This operation will come under mode 1.

$$\text{B1 as an alternative standby source} \begin{cases} SOC_1 >= 30\% \;||\; <= 96\%, \text{ set ref.} == 1 \\ SOC_2 == \text{ any value} \end{cases} \quad (2)$$

Due to any change on the load side or source side parameter at the K^{th} interval of time, renewable power may be sufficient to meet the load demand. In addition, there is a chance for a surplus of power at the source side; at that instant, battery 1 stops feeding to the load, and it acts as a storage unit. This process stays on l, repeating until SOC_1 becomes less than the minimum value.

Once the SOC_1 reaches its minimum value, the batteries will swap their role (see Equation (3)). Here, B1 acts as a storage device, and B2 acts as an alternative source. Those batteries will remain in their working mode until the SOC of B2 reaches its minimum value, i.e., 30% of its charge. In this mode, due to the load parameter or source, the side parameter

may adjust and just keep the system under a renewable-sourced mode for 'N' number of times. Nevertheless, the batteries will never change their mode until their own dual battery controller commands them. In this process, the batteries' charge cycle is reduced, which increases their lifetime. Figure 3 shows the flow chart of the dual battery algorithm, and Figure 4 shows the Simulink model of the dual battery controller unit. Table 1 has the logical parameters for entire system.

$$\begin{cases} \text{Set B2 as an alternative standby source} \\ \text{SOC}_1 < 30\% \,||\, \text{SOC}_2 >= 30\% \text{ set.ref.} == 0 \\ \text{SOC}_2 >= 30\%, \text{set.ref.} == 1 \end{cases} \quad (3)$$

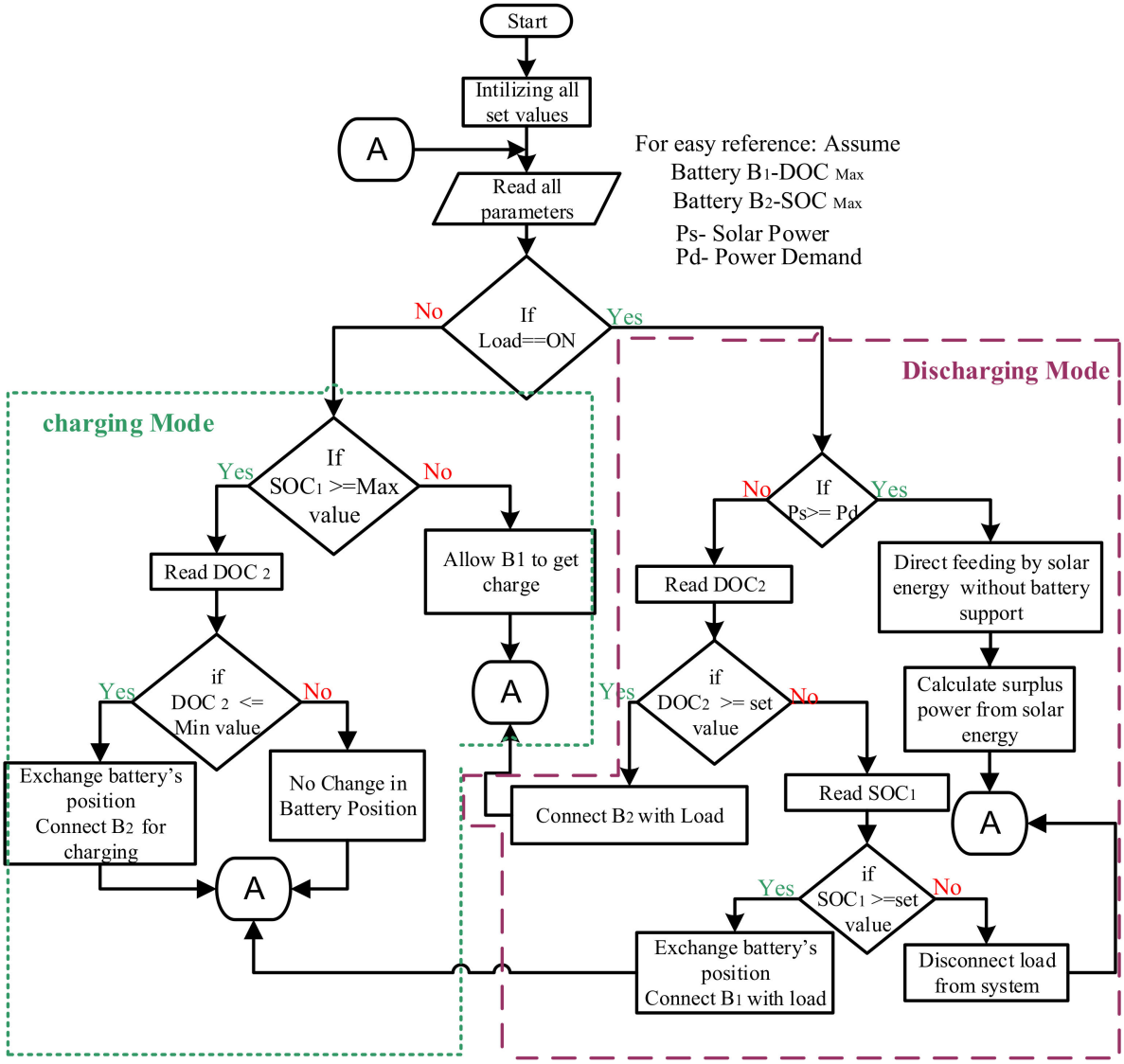

Figure 3. Flowchart of the dual battery storage system.

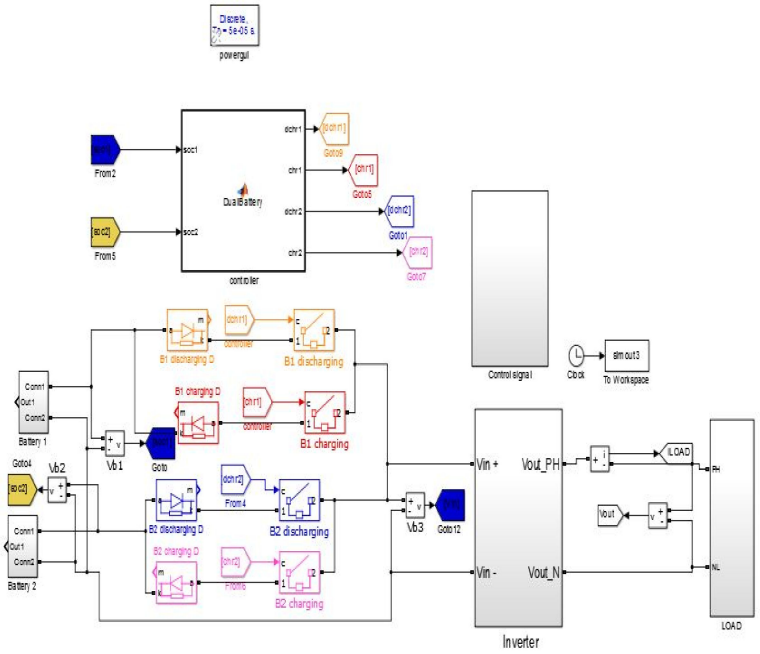

Figure 4. MATLAB Simulink diagram for the dual battery algorithm.

2.1. Dual Battery Mode 1 Operation

The circuit diagram of mode 1 is shown in Figure 5. In this mode, battery no. 1 is working as an alternative source to the load; on the other end, battery no. 2 behaves as a storage unit. In this mode, the diodes D1 and D4 operate in a forward bias; similarly, control switches S1 and S4 are closed. In this condition, battery no. 1 is always ready to feed the power to the load under any circumstances; likewise, battery no. 2 is also ready to store surplus power from renewable power source. The process of mode 1 will continue up to the condition when the SOC_1 reaches a minimum.

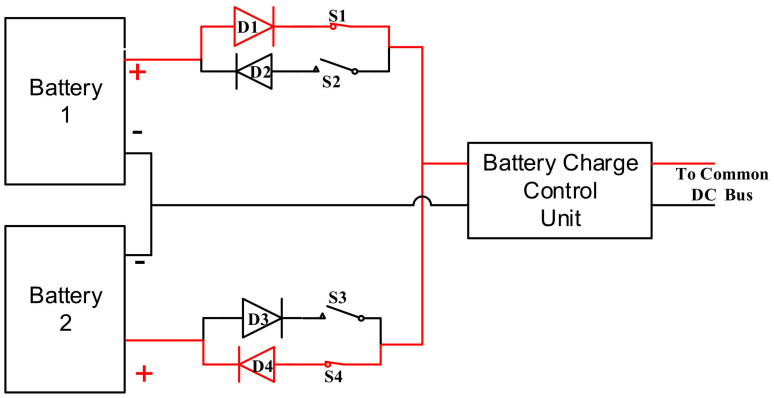

Figure 5. Circuit diagram of the dual battery mode 1 operation.

2.2. Dual Battery Mode-2 Operation

The circuit diagram of mode 2 is shown in Figure 6. In this mode, battery no. 2 is working as an alternative source to the load; on the other hand, battery no. 1 behaves as a storage unit. In this mode, diodes D2 and D3 operate in a forward bias; similarly, control switches S2 and S3 are closed, and the rest of the switches remain open. In this condition, the SOC of battery no. 2 may be between 30% and the maximum. Now, B2 is configured to feed power to the load under any circumstances; likewise, battery no. 1 is also ready to store the surplus power from a renewable power source. The process of mode 2 will

continue up to the situation when SOC2 reaches the minimum. The functional concept of the dual battery algorithm is expressed in Table 2.

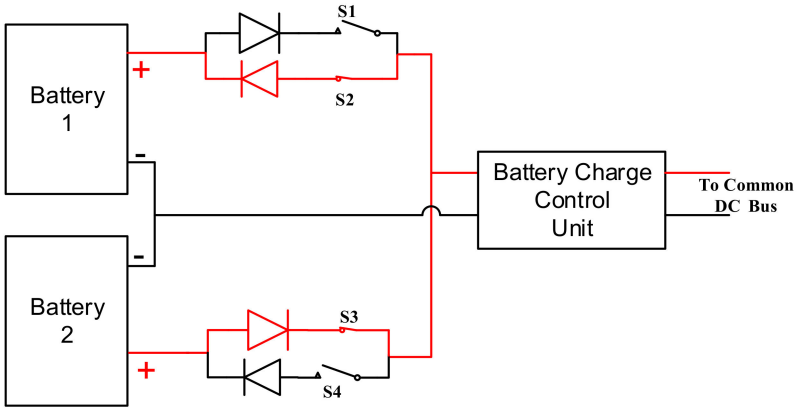

Figure 6. Circuit diagram of the dual battery mode 2 operation.

Table 2. Functional concept of the dual battery algorithm.

SOC Battery 1	SOC Battery 2	Pervious Load Status	Battery Support Requirement	DBS Algorithm	
				Output (Discharge)	Input (Charge)
Max	Max	Nil	Yes	Battery 1	Battery 2
Max	Max	Battery:1	No	-	Battery 2
Not Low	Max	Battery:1	Yes	Battery 1	Battery 2
Low	Max	Battery:1	Yes	Battery 2	Battery 1
Not Low	Max	Battery:2	No	-	Battery 1
Max	Not Low	Battery:2	Yes	Battery 2	Battery 1
Max	Low	Battery:1	Yes	Battery 1	Battery 2

From Figures 7 and 8, the illustrations clearly show that the SOC of the main battery has maintained an optimal way to remove the unwanted charge cycles. For instance, for the load ON position after 0.2 s but before 0.8 s, the main battery will remain constant on a charging model until it attains the maximum SOC or the auxiliary battery reaches its maximum DOC. Furthermore, the Figure 8 shows a better understanding for the above condition.

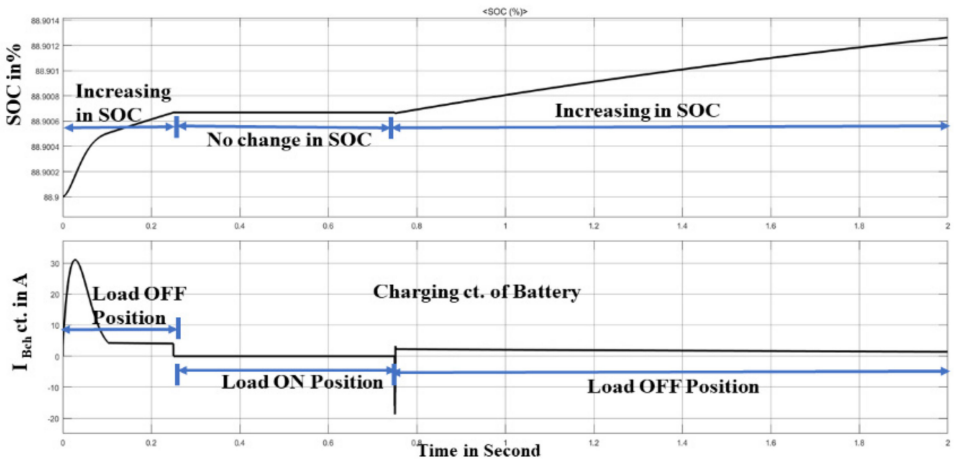

Figure 7. SOC and various load conditions for the main battery.

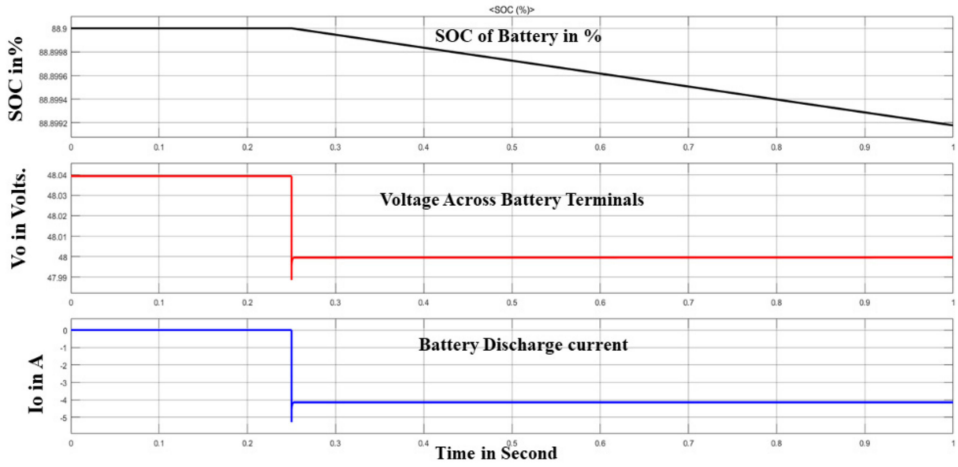

Figure 8. SOC and various load conditions for the auxiliary battery.

3. Modelling of Single Diode Cell PV

The proposed system is simulated by the MATLAB Simulink model using a lead-acid battery, and this study includes the various results, such as the modelling of a single diode solar PV, three-phase inverter. The PV model consists of a diode (D), shunt resistor (R_{sh}) and series resistor (R_s); in some cases, the high value of the shunt resistor can be negligible.

To improve the solar net power output, solar cells are connected with each other in a series and parallel the w.r.t load demand or generation capacity. The output current of the solar array is expressed as follows:

$$I = N_{ph}I_{ph} - N_{ph}\, I_o \left[\exp\left(q\left(\frac{\frac{V_{pv}}{N_s} + \frac{I_{pv}\, R_s}{N_p}}{dkT}\right)\right) - 1\right] - \frac{V_{pv}N_p}{N_s} + \frac{R_s I_{pv}}{R_{sh}} \quad (4)$$

Perturb and observe (hill climbing method) is the best and simplest approach to meet over the maximum power point tracking in the solar photovoltaic power generation method. The reason to justify P&O is that it requires a single voltage sensor to calculate the MPP value.

Solar MMPT Techniques

The proposed system is loaded with the P&O technique to avoid or reduce voltage fluctuation on the solar output terminal. One of the main reasons to implement this P&O is that it has a highly simple design and good accuracy when compared with the solar MPPT technique. The simulation results of the P&O method are discussed below. The actual voltage and current of the solar PV system is continuously monitored by a P&O controller; based on those values, the P&O controller generates gate pulses and sends them to the gate MPPT boost converter. Figure 9 shows the actual design of the P&O controller.

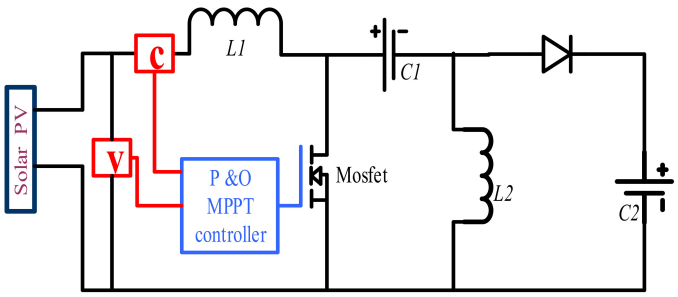

Figure 9. P&O-based MPPT boost converter design.

Figure 10 shows the voltage waveform and current waveform of the solar PV system. Similarly, Figure 11a shows the gate pulse of the MPPT DC-DC boost converter. The P&O controller compares the voltage reference value with the actual value of the solar output and decided the duty cycle of MPPT converter's gate pulse. The controller will make iteration for every pulse generation; moreover, the P&O controller is purely applying the new actual data for calculations. In simulation, the sine pulse width modulation (SPWM) is fused to obtain a smooth sine alternating voltage signal at inverter. Figure 11b shows the gate pulse of the inverter at various time divisions. It clearly explains switching sequences of the inverter with a proper timing interval. Figure 12 shows the inverter output voltage (V_o) and output current (I_o). Both I_o and V_o are mentioned in the graph; the SPWM inverter is producing a smooth AC voltage at its output terminal.

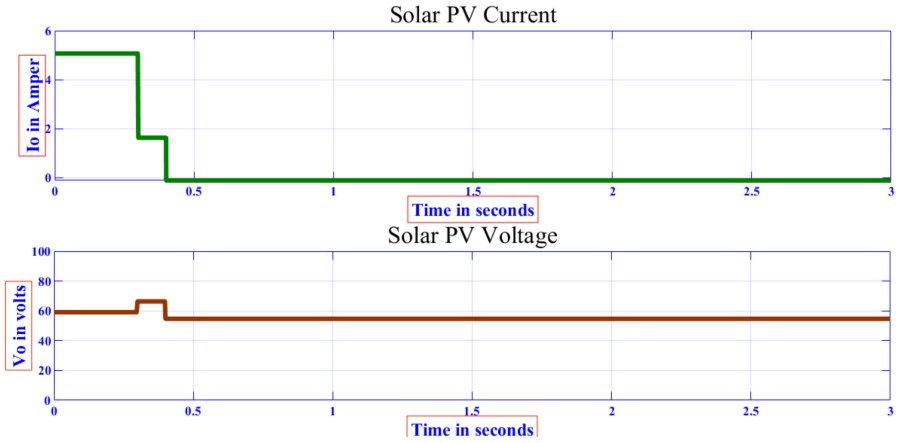

Figure 10. Output of the solar PV system.

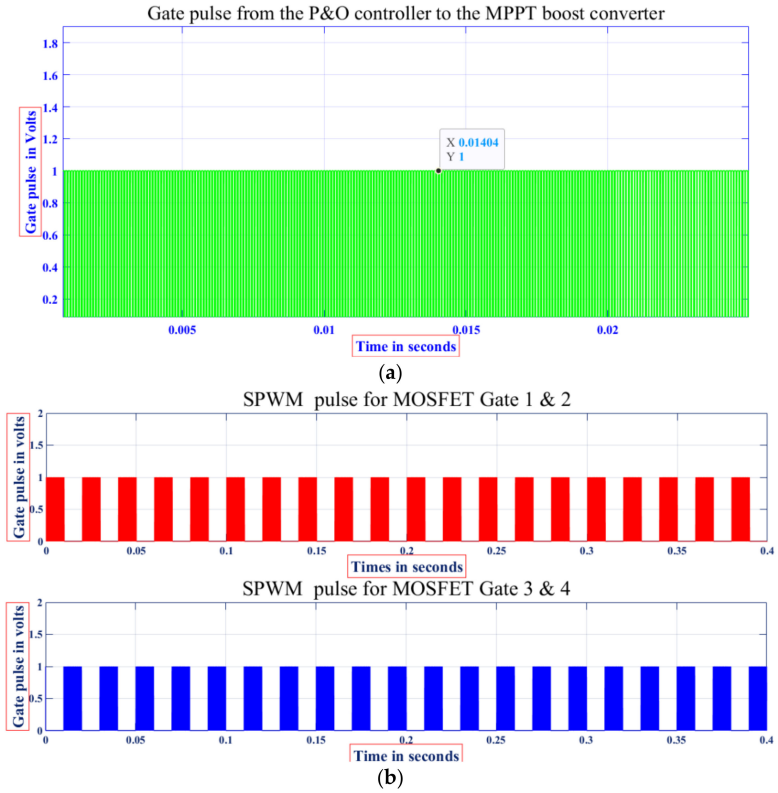

Figure 11. (**a**) Gate pulse of the P&O-based MPPT controller. (**b**) Inverter gate pulses.

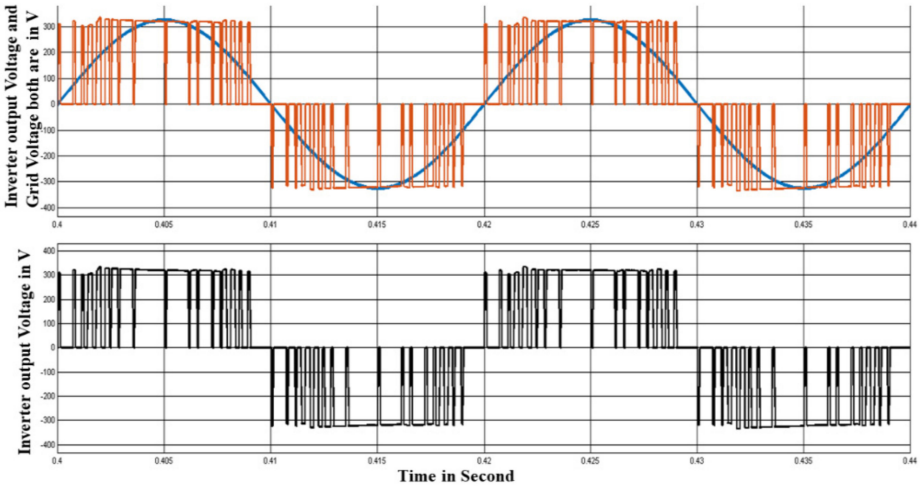

Figure 12. SPWM inverter output voltage with grid synchronization.

4. Control Circuit and Driver Circuit

The dsPIC 30f4011 is used as a main controller for this proposed system, clearly shown in Figure 13. It is a 40-pin controller; it has features such as a modified Harvard architecture, high-performance modified RISC CPU with a DSP engine, 16-bit controller, three pairs of inbuilt PWM chambers, 10-bit ACD accuracy with a conversion rate at 500 Ksps, operation at 30MIPS, five 16-bit programmable timer/counter and 30 interrupt sources.

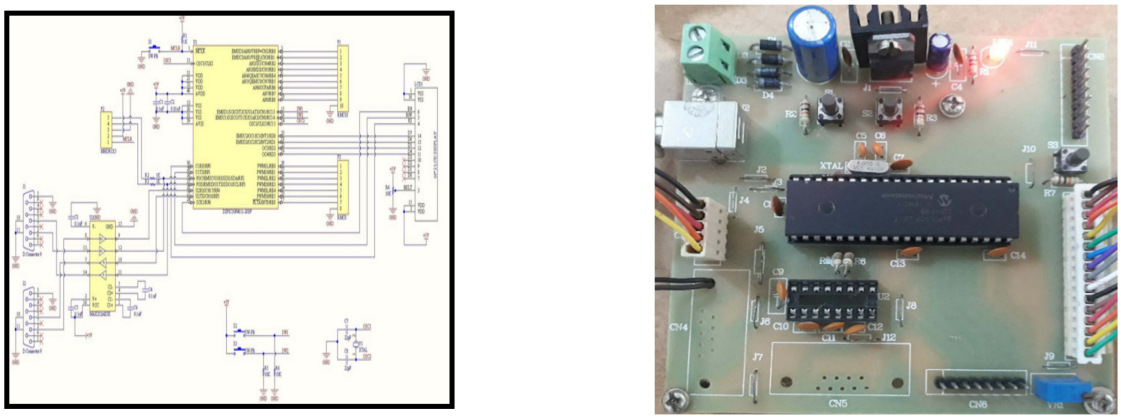

(**a**) (**b**)

Figure 13. (**a**) Schematic layout of the dsPIC 30f4011 controller; (**b**) real hardware circuit of the dsPIC 30f4011 controller board.

Designing of Driver Circuit

Normally, the proposed main controller (dsPIC 30F 4011) operates in the voltage range of 4.5 to 5.5 volts, and its control signals are also within the same voltage ranges. The power electronics switches (IRF740) require a minimum of 12v for the gate pulse. Figure 14a shows the general block diagram of gate signals' flow path. Initially, the main controller produces the gate signal at a prescribed port pin according to the program. The control signals were directly connected with a opto-coupler (Sfh615a) for the electrical isolation purpose.

It will protect the main controller from damage because of a power circuit failure or short circuit in the power circuit condition. The output of the opto-coupler is inverse to the actual signals that are produced by the main controller. Inverted gate pulses are applied to the buffer (HEF4050B); it clears the ripples from the gate pulse. The ripples in the gate pulses generate harmonics at the inverter output. A driver circuit is used to interface these control and power circuits for which two low-power MOSFETs (IRF9250 and IRFZ44) are

used in the driver circuit, which drives a power MOSFET (IRF460). Figure 14c shows the circuit diagram of the driver circuit, and in Figure 15b, a photograph of the driver circuit with electrical isolation protection is shown. Here, there is no need to use a boost trap capacitor.

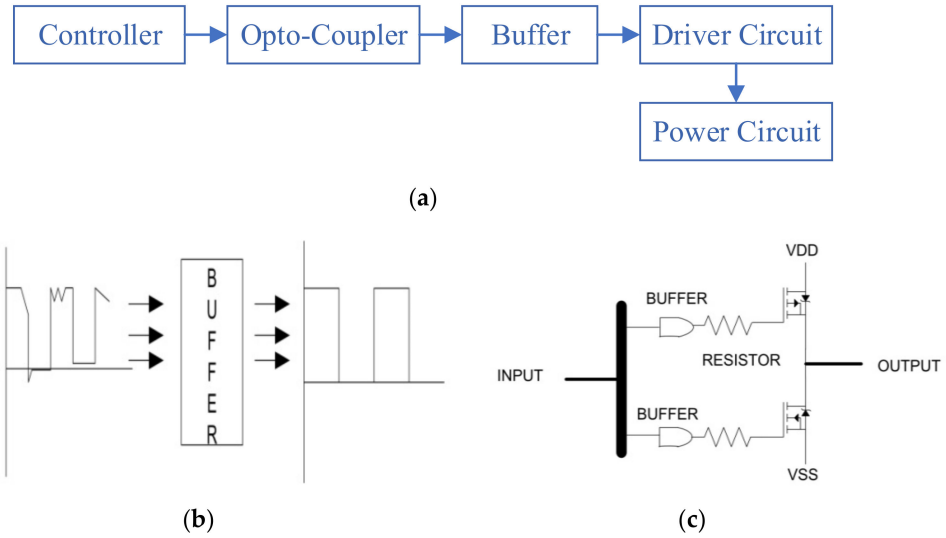

Figure 14. (**a**) Flowchart for the interfacing power circuit; (**b**) buffer i/p and o/p waveform of the buffer circuit; (**c**) circuit diagram of the driver circuit.

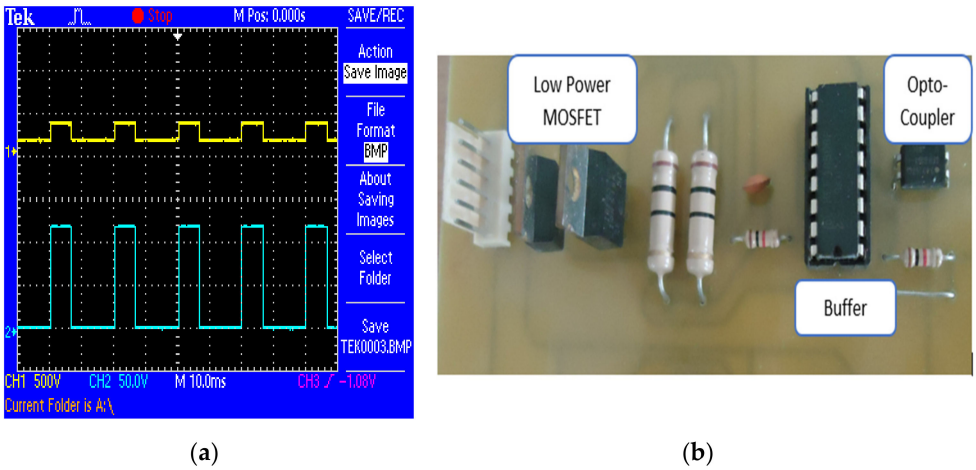

Figure 15. (**a**). Driver input and output, 14. (**b**). Signal Photograph of driver circuit.

The entire hardware processes are carried out with neat, expected results; a single-layer printed circuited board (PCB) is used in all hardware circuits. All components in this system belongs to the dual-in-line package category.

The schematic circuit of the three-phase inverter and its real photograph are shown in Figure 16. The inverter is designed as a three-arm, three-phase and three-wire inverter. Here, power MOSFETs (IRFP460) were used to design the inverter circuit along with a RC snubber to protect from any sudden change in voltage (dv/dt) and current (di/dt). The input of this inverter is fed by a common DC bus, which is connected with a dual battery and with a renewable power source (solar PV system). Figure 17a shows the real-time programming environmental setup; a dsPIC from the microchip family is used as a main controller, and a pickit3 is used as a program dump tool.

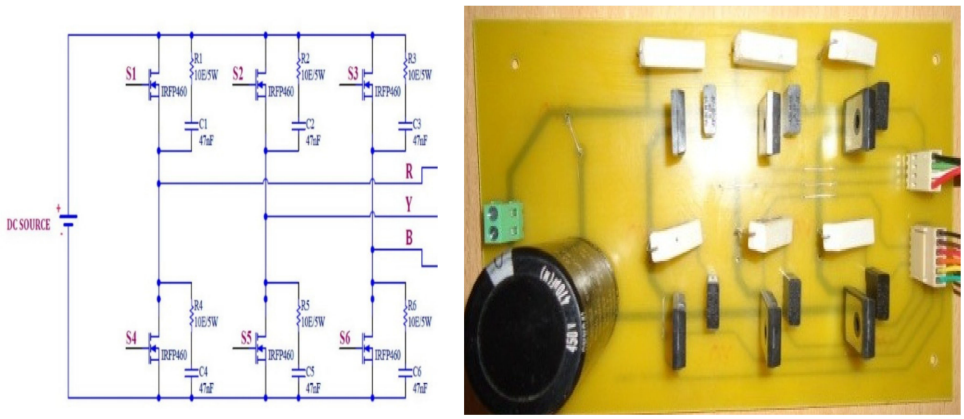

(**a**) (**b**)

Figure 16. (**a**) Schematic circuit of the three-phase inverter; (**b**) a real photograph of the inverter.

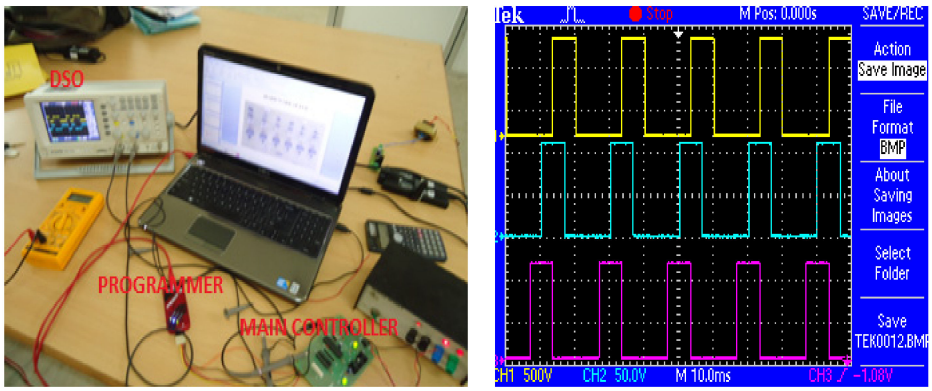

(**a**) (**b**)

Figure 17. (**a**) Real-time programming environment; (**b**) gate pulse for the three-phase inverter.

Similarly, Figure 16b shows the gate pulse of the inverter at different K^{th} intervals of time. Instead of IRF240, low-power MOSFETs are used as driver circuits. The dead time between the outgoing switch and incoming switches are calculated manually and controlled via programming. Finally, Figure 18 deals with the three-phase inverter output, the final output of this proposed system; Figure 18a shows the voltages across a two-phase, no-load condition, and Figure 18b shows the same inverter output with the load condition.

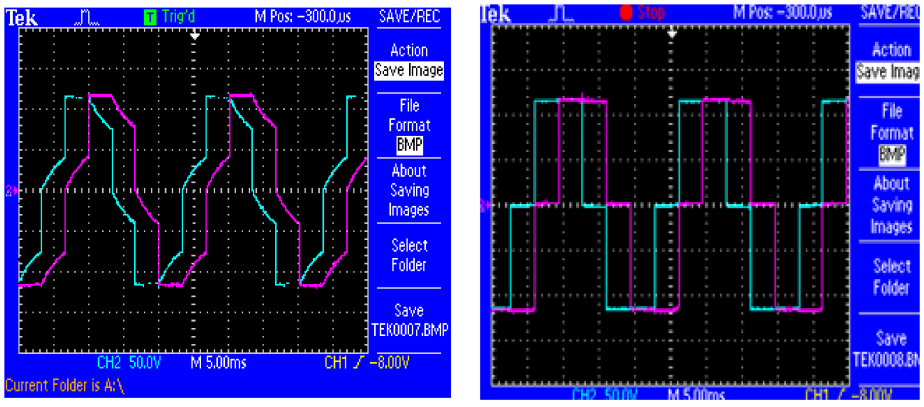

(**a**) (**b**)

Figure 18. Inverter outputs at various load conditions.

The proposed model enhances the lifetime of the battery by avoiding an unwanted charge cycle. During discharging, the oxidation takes place, and, therefore, lead sulphate is deposited on the anode; lead 4+ loses 2 electrons, so it forms lead 2+ ions, and here, also, lead sulphate (PbO2) is deposited on the cathode. Similarly, during charging, the lead sulphate, which is deposited on the cathode, is converted back to lead peroxide (PbO2), and the anode layer lead sulphate (PbSO4) is converted into a sponge (porous) and lead (Pb). Thus, the charging and discharging happens with a slighter time interval, directly reducing the number of battery charge cycles and further reducing the lifetime of the battery. Therefore, the proposed system improves the lifetime of the battery by reducing the ineffective charge cycle.

5. Conclusions

The proposed paper has presented a dual battery storage system with the MPPT technique to improve the efficiency of solar PV. In addition, the dual battery storage system introduced a new concept for storage systems; it was simulated by using the MATLAB Simulink model. Additionally, a real-time, three-phase inverter was designed with a high protection circuit. Their (protection circuit) results were discussed with its output waveforms, in which low-power MOSFETs are used as driver circuits to drive the power MOSFET; dead time is controlled by a switching program, and RC snubber protection is also implemented to the power switch. The overall performance of the proposed system is a highly recommended because it enriches the lifetime of battery and high-protection circuit.

Author Contributions: Conceptualization, V.B.T.R.; methodology, S.R.G.; validation, D.K. and M.R.; formal analysis, R.S.; writing—original draft preparation, V.B.T.R.; writing—review and editing, M.R. and S.S.A.; supervision, A.D. and Y.A.; funding acquisition, Y.A. All authors have read and agreed to the published version of the manuscript.

Funding: Taif University Researchers Supporting Project number (TURSP-2020/161), Taif University, Taif, Saudi Arabia.

Institutional Review Board Statement: Not applicable.

Informed Consent Statement: Not applicable.

Data Availability Statement: Data will be made available on request from the corresponding author.

Acknowledgments: The authors would like to thank Taif University Researchers Supporting Project number (TURSP-2020/161), Taif University, Taif, Saudi Arabia for supporting this work.

Conflicts of Interest: The authors declare no conflict of interest.

References

1. Kim, K.; Cha, H.; Kim, H.-G. A New Single-Phase Switched-Coupled-Inductor DC–AC Inverter for Photovoltaic Systems. *IEEE Trans. Power Electron.* **2017**, *32*, 5016–5022. [CrossRef]
2. Babaei, E.; Asl, E.S.; Babayi, M.H. Steady-State and Small-Signal Analysis of High-Voltage Gain Half-Bridge Switched Boost Inverter. *IEEE Trans. Ind. Electron.* **2016**, *63*, 3546–3553. [CrossRef]
3. Li, Y.; Du, S.; Zhang, T.; Tan, X. Model Predictive PWM for Hybrid Active Power Filter. *AMSE J.-AMSE IIETA* **2017**, *90*, 98–116. [CrossRef]
4. Sikkabut, S.; Mungporn, P.; Ekkaravarodome, C.; Bizon, N.; Tricoli, P.; Nahid-Mobarakeh, B.; Davat, B.; Thounthong, P. Control of High-Energy High-Power Densities Storage Devices by Li-ion Battery and Super capacitor for Fuel Cell/Photovoltaic Hybrid Power Plant for Autonomous System Applications. *IEEE Trans. Ind. Appl.* **2016**, *52*, 4395–4407. [CrossRef]
5. Yang, H.; Qin, T.; Deng, T.; Zhang, W.; Zheng, W. Rationalizing the Anion Storage in Cathodes for Optimum Dual-Ion Batteries: State of the Art and the Prospect. *Energy Fuels* **2020**, *34*, 15701–15713. [CrossRef]
6. Shi, X.; Zhang, W.; Wang, J.; Zheng, W.; Huang, K.; Zhang, H.; Seng, S.; Chen, H. (EMIm)+(PF6)−ionic liquid unlocks optimum energy/power density for architecture of nanocarbon-based dual-ion battery. *Adv. Energy Mater.* **2016**, *24*, 1601378. [CrossRef]
7. Ram, J.P.; Rajasekar, N. A Novel Flower Pollination Based Global Maximum Power Point Method for Solar Maximum Power Point Tracking. *IEEE Trans. Power Electron.* **2017**, *32*, 8486–8499. [CrossRef]
8. Oladipo, S.; Sun, Y.; Wang, Z. An enhanced flower pollinated algorithm with a modified fluctuation rate for global optimisation and load frequency control system. *IET Renew. Power Gener.* **2022**. [CrossRef]

9. Kumar, N.; Hussain, I.; Singh, B.; Panigrahi, B.K. Single sensor based MPPT for partially shaded solar photovoltaic by using human psychology optimisation algorithm. *IET Gener. Transm. Distrib.* **2017**, *11*, 2562–2574. [CrossRef]
10. Thurai Raaj, V.B.; Suresh, K.; Srinivasa Rao, G. Applying Three Port Converter with Dual Battery Storage System for Hybrid Power Generation. *J. Sci. Ind. Res.* **2020**, *79*, 640–646.
11. Ramyar, A.; Iman-Eini, H.; Farhangi, S. Global Maximum Power Point Tracking Method for Photovoltaic Arrays Under Partial Shading Conditions. *IEEE Trans. Ind. Electron.* **2017**, *64*, 2855–2864. [CrossRef]
12. Merhi, H.; Fell, A.; Grübel, B.; Glatthaar, M.; Kluska, S. Inhomogeneity of Plated Contacts for c-Si Solar Cells and Their Impact on Solar Cell Efficiency. *IEEE J. Photovolt.* **2020**, *10*, 1455–1462. [CrossRef]
13. Nabulsi, A.; Dhaouadi, R. Efficiency Optimization of a DSP-Based Standalone PV System Using Fuzzy Logic and Dual-MPPT Control. *IEEE Trans. Ind. Inform.* **2012**, *8*, 573–584. [CrossRef]
14. Echalih, S.; Abouloifa, A.; Lachkar, I.; El Aroudi, A.; Hekss, Z.; Giri, F.; Al-Numay, M.S. A Cascaded Controller for a Grid-Tied Photovoltaic System with Three-Phase Half-Bridge Interleaved Buck Shunt Active Power Filter: Hybrid Control Strategy and Fuzzy Logic Approach. *IEEE J. Emerg. Sel. Top. Circuits Syst.* **2022**, *12*, 320–330. [CrossRef]
15. Guisández Hernández, A.; Santos, S.P. Modelling and Experimental Validation of Aging Factors of Photovoltaic Solar Cells. *IEEE Lat. Am. Trans.* **2021**, *19*, 1270–1277. [CrossRef]
16. Wang, W.; Song, Q.; Li, Y.; Zhang, N. A dual fuzzy logic controller-based active thermal control strategy of SiC power inverter for electric vehicles. *IET Electr. Power Appl.* **2022**, *16*, 190–205. [CrossRef]
17. Li, X.; Wen, H.; Jiang, L.; Xiao, W.; Du, Y.; Zhao, C. An Improved MPPT Method for PV System with Fast-Converging Speed and Zero Oscillation. *IEEE Trans. Ind. Appl.* **2016**, *52*, 5051–5064. [CrossRef]
18. Fard, M.T.; Khan, W.A.; He, J.; Weise, N.; Abarzadeh, M. Fast online diagnosis of open-circuit switching faults in flying capacitor multilevel inverters. *Chin. J. Electr. Eng.* **2020**, *6*, 53–62. [CrossRef]
19. Mansour, R.B.; Khan, M.A.M.; Alsulaiman, F.A.; Mansour, R.B. Optimizing the Solar PV Tilt Angle to Maximize the Power Output: A Case Study for Saudi Arabia. *IEEE Access* **2021**, *9*, 15914–15928. [CrossRef]
20. Leena, N.; Durai Raj, B.; Gunabalan, R. Computer-based laboratory teaching tools: An overview of LabVIEW and MATLAB. In Proceedings of the 2012 IEEE International Conference on Engineering Education: Innovative Practices and Future Trends (AICERA), Kottayam, India, 19–21 July 2012; pp. 1–6. [CrossRef]
21. Singh, B.; Jain, C. A Decoupled Adaptive Noise Detection Based Control Approach for a Grid Supportive SPV System. *IEEE Trans. Ind. Appl.* **2017**, *53*, 4894–4902. [CrossRef]
22. Guo, L.; Xu, Z.; Li, Y.; Chen, Y.; Jin, N.; Lu, F. An Inductance Online Identification-Based Model Predictive Control Method for Grid-Connected Inverters with an Improved Phase-locked Loop. *IEEE Trans. Transp. Electrif.* **2021**. [CrossRef]
23. Liu, T.; Sun, Y.; Liu, Y.; Gui, Y.; Zhao, Y.; Wang, D.; Shen, C. Abnormal traffic-indexed state estimation: A cyber–physical fusion approach for Smart Grid attack detection. *Future Gener. Comput. Syst.* **2015**, *49*, 94–103. [CrossRef]
24. Abdelhakim, A.; Mattavelli, P.; Spiazzi, G. Three-Phase Split-Source Inverter (SSI): Analysis and Modulation. *IEEE Trans. Power Electron.* **2016**, *31*, 7451–7461. [CrossRef]
25. Zhang, M.; Liang, R.; Yang, N.; Gao, R.; Zheng, Y.; Deng, Y.; Hu, Y.; Yu, A.; Chen, Z. Eutectic Etching toward In-Plane Porosity Manipulation of Cl-Terminated MXene for High-Performance Dual-Ion Battery Anode. *Adv. Energy Mater.* **2022**, *12*, 2102493. [CrossRef]
26. Meng, Y.-F.; Liang, H.-J.; Zhao, C.-D.; Li, W.-H.; Gu, Z.-Y.; Yu, M.-X.; Zhao, B.; Hou, X.-K.; Wu, X.-L. Concurrent recycling chemistry for cathode/anode in spent graphite/$LiFePO_4$ batteries: Designing a unique cation/anion-co-workable dual-ion battery. *J. Energy Chem.* **2022**, *64*, 166–171. [CrossRef]
27. Zafar, Z.A.; Abbas, G.; Knizek, K.; Šilhavík, M.; Kumar, P.; Jiricek, P.; Houdkova, J.; Frank, O.; Cervenka, J. Chaotropic Anion Based "Water-in-Salt" Electrolyte Realizes a High Voltage Zn–Graphite Dual-Ion Battery. *J. Mater. Chem. A* **2022**. [CrossRef]
28. Malinowski, M.; Leon, J.I.; Abu-Rub, H. Solar Photovoltaic and Thermal Energy Systems: Current Technology and Future Trends. *Proc. IEEE* **2017**, *105*, 2132–2146. [CrossRef]
29. Kumar, V.; Singh, S.; Jain, S. A Reduced Switch Count Symmetric T-type Multilevel Inverter with Single and Multiple Switch Open Circuit Fault Tolerant Capabilities. *IETE J. Res.* **2022**, 1–23. [CrossRef]
30. Zhao, Z.; Wang, T.; Benbouzid, M. A fault-tolerant reconfiguration system based on pilot switch for grid-connected inverters. *Microelectron. Reliab.* **2022**, *131*, 114511. [CrossRef]
31. Yang, Y.; Sangwongwanich, A.; Blaabjerg, F. Design for reliability of power electronics for grid-connected photovoltaic systems. *CPSS Trans. Power Electron. Appl.* **2016**, *1*, 92–103. [CrossRef]
32. Jin, Y.; Xiao, Q.; Jia, H.; Ji, Y.; Dragicevic, T.; Teodorescu, R.; Blaabjerg, F. A Novel Detection and Localization Approach of Open-Circuit Switch Fault for the Grid-Connected Modular Multilevel Converter. *IEEE Trans. Ind. Electron.* **2022**. [CrossRef]
33. Tuckey, A.; Round, S. Grid-Forming Inverters for Grid-Connected Microgrids: Developing "good citizens" to ensure the continued flow of stable, reliable power. *IEEE Electrif. Mag.* **2022**, *10*, 39–51. [CrossRef]
34. Long, B.; Shen, D.; Cao, T.; Rodriguez, J.; Guerrero, J.M.; Garcia, C.; Kil, T.C. Power Losses Reduction of T-type Grid-Connected Converters Based on Tolerant Sequential Model Predictive Control. *IEEE Trans. Power Electron.* **2022**. [CrossRef]